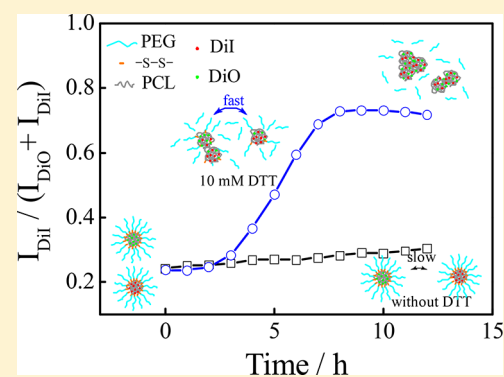


Effect of Hydrophobic Chain Length on the Stability and Guest Exchange Behavior of Shell-Sheddable Micelles Formed by Disulfide-Linked Diblock Copolymers

Haiyan Fan,[†] Yixia Li,[†] Jinxian Yang,[†] and Xiaodong Ye^{*,†,‡,§}[†]Hefei National Laboratory for Physical Sciences at the Microscale, Department of Chemical Physics and [‡]CAS Key Laboratory of Soft Matter Chemistry, University of Science and Technology of China, Hefei, Anhui 230026, China

Supporting Information

ABSTRACT: Reduction-responsive micelles hold enormous promise for application as drug carriers due to the fast drug release triggered by reducing conditions and high anticancer activity. However, the effect of hydrophobic chain length on the stability and guest exchange of reduction-responsive micelles, especially for the micelles formed by diblock copolymers containing single disulfide group, is not fully understood. Here, shell-sheddable micelles formed by a series of disulfide-linked copolymer poly(ethylene glycol)-*b*-poly(ϵ -caprolactone) (PEG–SS–PCL) containing the same chain length of PEG but different chain lengths of hydrophobic block PCL were prepared and well characterized. The influence of the chain length of hydrophobic PCL block on the stability and guest exchange of PEG–SS–PCL micelles was studied by the use of both dynamic laser light scattering (DLS) and fluorescence resonance energy transfer (FRET). The results show that longer PCL chains lead to a slower aggregation rate and guest exchange of micelles in the aqueous solutions containing 10 mM dithiothreitol (DTT). The cell uptake of the shell-sheddable PEG–SS–PCL micelles in vitro shows that the amount of internalization of dyes loaded in PEG–SS–PCL micelles increases with the chain length of hydrophobic PCL block investigated by flow cytometric analysis and confocal fluorescence microscopy.



INTRODUCTION

It is well-known that self-assembly of amphiphilic block copolymers into polymeric micelles and vesicles can provide hydrophobic regions and/or hydrophilic cavities to encapsulate hydrophobic and/or hydrophilic drugs.^{1,2} These nanocarriers have received much attention over the last three decades due to an ability to prolong the circulation time of drugs in the blood and to accumulate in tumor tissues because of the enhanced permeability and retention (EPR) effect, which could also reduce side effects of anticancer drugs.^{3–7} Moreover, stimuli-responsive polymer micelles have been designed to trigger the release of drugs and enhance the therapeutic efficiency.^{8–11} In particular, micelles and nanogels formed from reduction-responsive polymer with monofunctional disulfide group or multifunctional disulfide groups have been shown to promote drug delivery in cancer cells, presumably due to the higher concentration of the reducing agent glutathione (GSH) in the cell interior (2–10 mM) than the extracellular environments (2–10 μ M).^{12–38} For example, Zhong and co-workers reported that shell-sheddable micelles formed from block copolymers containing only one disulfide group between hydrophilic block and hydrophobic block released doxorubicin (DOX) much faster inside cells and showed a higher antitumor efficacy as compared to reduction insensitive micelles.^{13–15} They also found that dual-responsive biodegradable micelles and functionalized reduction-sensitive micelles exhibited superior

tumor growth inhibition.^{17–20} Wang and co-workers reported that shell-detachable micelles assembled from a single disulfide-linked copolymer of poly(ϵ -caprolactone) and poly(ethylene phosphate) (PCL–SS–PEEP) displayed reduction-responsive release and faster intracellular DOX release.²¹ Oh and co-workers prepared a series of shell-sheddable micelles based on hydrophobic polylactide (PLA) block that exhibited enhanced release of encapsulated drugs from micelles.^{22–24}

Although different reduction-sensitive micelles have been synthesized and characterized, the stability and guest exchange of these micelles are not well understood, in particular, for the micelles formed from diblock copolymers containing a single disulfide group.^{13,14,21,30} Until now, to the best of our knowledge, only a few studies have been done on the mechanism of the release of loaded compounds and drugs and guest exchange of the reduction-sensitive micelles.^{31,32} For example, Cheng et al. studied the stability of disulfide bonded poly(ethylene glycol)-(cysteine)₄-poly(D,L-lactic acid) (PEG-(Cys)₄-PDLLA) in the bloodstream and they found that the reduction-sensitive micelles have a higher stability after systemic administration compared to the reduction-insensitive micelles using fluorescence resonance energy transfer (FRET)

Received: June 23, 2017

Revised: August 29, 2017

Published: September 19, 2017

methods.³¹ It is well-known that there is a pair of dyes in FRET methods and one dye acts as the energy donor and the other serves as the energy acceptor. When the distance between the two dyes is comparable to the Förster radius, energy transfer may occur if the fluorescence emission spectrum of the donor overlaps the absorption spectrum of the acceptor.^{39–41} Recently, this method has also been used to study the stability and release behavior of micelles formed by reduction insensitive block copolymers in vitro and in vivo.^{42–57} Moreover, Thayumanavan et al. utilized FRET to investigate the stability and guest exchange of cross-linked polymer nanogels and recently they found that the mechanism of guest change in the pH-sensitive nanogels can change between collision-based mechanism and diffusion-based mechanism based on the microenvironment of the nanogel interior.^{26,27,44,45}

In this work, the effect of the chain length of the hydrophobic block (PCL) on the stability and guest exchange of the micelles formed by disulfide-linked copolymer PEG–SS–PCL was studied by a combination of FRET method and laser light scattering. Moreover, we also used flow cytometric analysis and confocal fluorescence microscopy to investigate the influence of chain length of PCL segment on the cellular uptake of PEG–SS–PCL micelles in vitro and related dyes release kinetics from these micelles.

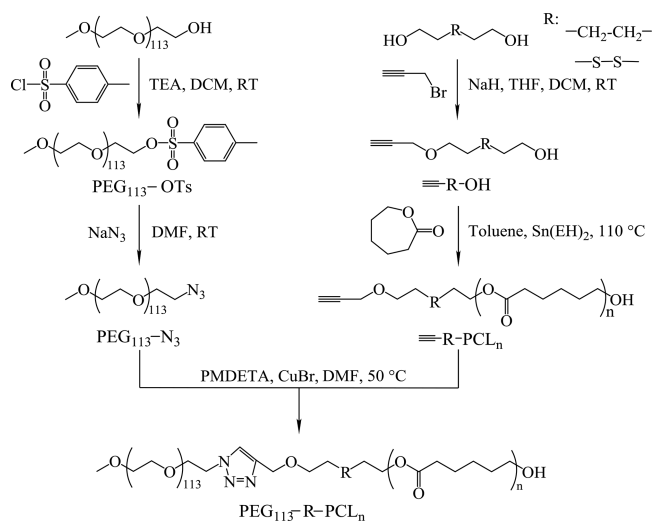
MATERIALS AND METHODS

Poly(ethylene glycol) methyl ether (PEG₁₁₃–OH, $M_n = 5000$ g/mol, Aldrich) was dried by azeotropic distillation from toluene before each reaction. ϵ -Caprolactone (CL, Aladdin, 99%) was purified by distilling under reduced pressure over calcium hydride. Sodium azide (NaN₃, Sigma-Aldrich, 99%), *p*-benzenesulfonyl chloride (TsCl, Alfa Aesar, 98%), 1,6-hexanediol (Ourchem, 96.5%), 2-hydroxyethyl disulfide (Aldrich, 90%), propargyl bromide (Aladdin, 97%), sodium hydride (NaH, Aladdin, 80%), *N,N,N',N',N''*-pentamethyldiethylenetriamine (PMDETA, Sigma-Aldrich, 99%), stannous octoate (Sn(EH)₂, Sigma-Aldrich, 95%), 3,3'-dioctadecyl-oxocarbocyanine perchlorate (DiO, Beyotime), 1,1'-dioctadecyl-3,3,3',3'-tetramethylindocarbocyanine perchlorate (DiI, Beyotime), and dithiothreitol (DTT, Aladdin, 99%) were used directly as received without further purification. Dimethylformamide (DMF, Sinopharm, 97%) was purified by distilling under a reduced pressure after dried over anhydrous magnesium sulfate. Dichloromethane (DCM, Sinopharm, 97%) and triethylamine (TEA, Sinopharm, 99%) were distilled over CaH₂. Tetrahydrofuran (THF, Sinopharm, 97%) and toluene (Sinopharm, 97%) were distilled over metal sodium using benzophenone as an indicator.

The synthesis of PEG–SS–PCL is described in detail as follows, as shown in Scheme 1, and the synthesis of PEG–CC–PCL is similar.

Synthesis of PEG₁₁₃–tosylate (PEG₁₁₃–OTs). *p*-Benzenesulfonyl chloride (TsCl) (7.63 g, 40.00 mmol) were dissolved in dichloromethane (DCM, 50 mL). Under nitrogen protection the TsCl solution was added into a DCM (50 mL) solution containing poly(ethylene glycol) methyl ether (20.00 g, 4.00 mmol) and triethylamine (TEA, 5.30 mL, 40.00 mmol) at 0 °C and within 0.5 h. The reaction was stopped after stirring for 24 h at room temperature with the addition of 100 mL of water. The mixture was diluted with DCM (100 mL) and washed with 1 M hydrochloric acid (HCl) solution (80 mL) followed by saturated sodium chloride aqueous solution (80 mL) for three times. Then the DCM solution was dried over

Scheme 1. Synthetic Pathways for PEG–SS–PCL and PEG–CC–PCL



anhydrous sodium sulfate. The solvent DCM was removed by rotary evaporation. The crude product was dissolved in THF (50 mL), then precipitated into an excess of cold diethyl ether and collected by filtration. The purification process was repeated twice. Finally, the polymer (PEG₁₁₃–OTs, 13.60 g) was acquired by filtration and dried in a vacuum oven at room temperature in a 68% yield.

Synthesis of PEG₁₁₃–N₃. The synthetic method of PEG₁₁₃–N₃ by azidation has been published previously.^{58,59} PEG₁₁₃–OTs (5.00 g, 1.00 mmol) and sodium azide (1.30 g, 20.00 mmol) were dissolved in purified DMF (80 mL). The reaction mixture was stirred at 30 °C for 30 h. After removing the solvent DMF under reduced pressure, the mixture was diluted with THF. Following by centrifugation at 4000 rpm at room temperature for 30 min, the supernatant liquid was precipitated into an excess of cold diethyl ether. The product (PEG₁₁₃–N₃, 4.85 g) was collected by filtration and dried in a vacuum oven in a 97% yield.

Synthesis of the Initiator ≡–SS–OH. The initiator of ring-opening polymerization of ϵ -caprolactone was synthesized according to our previous work as follows.⁶⁰ 2-Hydroxyethyl disulfide (29.94 g, 175.00 mmol) was dissolved in the mixed solvents of purified THF (150 mL) and DCM (150 mL) at room temperature. Then NaH powder (4.38 g, 145.83 mmol) was added to the reaction in three consecutive portions under nitrogen atmosphere at 0 °C within 3 h. The reaction mixture was stirred at room temperature for another 1 h. Under nitrogen protection, THF solution (150 mL) containing propargyl bromide (13.76 g, 116.67 mmol) was added into the reaction mixture within 1 h. The reaction was stopped after stirring for 7 h at room temperature with the addition of a few drops of water. Then the mixture was filtered and dried over anhydrous sodium sulfate. The solvent was removed by rotary evaporation. The crude product was purified by column chromatography on silica gel (eluent: *n*-hexane/ethyl acetate 10:1 to 5:1) to give a pale-yellow clear oil (≡–SS–OH, 11.30 g) in a 50% yield.

Synthesis of ≡–SS–PCL. ≡–SS–PCL with different molar masses was synthesized through ring-opening polymerization using ≡–SS–OH as an initiator and Sn(EH)₂ as a catalyst.⁶¹ For example, the procedure of the synthesis of ≡–SS–PCL₃₉ ($M_n = 4.6 \times 10^3$ g/mol) is outlined as follows. ≡–SS–OH

(0.1152 g, 0.60 mmol) and $\text{Sn}(\text{EH})_2$ (0.0486 g, 0.12 mmol) were dissolved in purified toluene (30 mL) in a three-necked, round-bottomed flask under a nitrogen atmosphere at 110 °C. Then, ϵ -caprolactone (3.00 g, 26.30 mmol) was added into the reaction quickly. The reaction mixture was stirred at 110 °C for another 10 h under reflux. After removing the solvent toluene under reduced pressure, the remaining portion was diluted with THF, then precipitated into an excess of cold diethyl ether. The polymer ($\equiv\text{-SS-PCL}_{39}$, $M_n = 4.6 \times 10^3$ g/mol, 2.55 g) was obtained by filtration and dried in a vacuum oven in an 85% yield. $\equiv\text{-SS-PCL}$ with other number-average molar masses of 2.7×10^3 and 7.1×10^3 g/mol were synthesized through the same procedure using different ratios of monomer to the initiator.

Synthesis of PEG-SS-PCL. The block copolymer was synthesized by click chemistry.^{62,63} For example, the procedure of the synthesis of $\text{PEG}_{113}\text{-SS-PCL}_{39}$ is outlined as follows. $\text{PEG}_{113}\text{-N}_3$ (0.5000 g, 0.10 mmol), $\equiv\text{-SS-PCL}_{39}$ (0.4800 g, 0.10 mmol), and PMDETA (0.0173 g, 0.10 mmol) were dissolved in DMF (10 mL) and degassed via three freeze-pump-thaw cycles. CuBr (0.0154 g, 0.10 mmol) was rapidly added to the mixture using a small hot funnel. The reaction was heated to 50 °C and stirred for 48 h. After that, the reaction mixture was passed through neutral alumina to remove metal salt using THF as the eluent. After removing the excess solvent, the block copolymer was precipitated into an excess of cold diethyl ether and collected by filtration. The final product ($\text{PEG}_{113}\text{-SS-PCL}_{39}$, 0.9114 g) was acquired after drying in a vacuum oven in a 93% yield. The unreacted $\equiv\text{-SS-PCL}_{39}$ was removed by the click chemistry with excessive azide resin.⁶⁴ The copolymer (0.1000 g, 0.01 mmol), the azide resin (0.0034 g azide group 0.01 mmol/g), and PMDETA (0.0017 g, 0.01 mmol) were added in DMF (2 mL), and the mixture was degassed via three freeze-pump-thaw cycles. CuBr (0.0015 g, 0.01 mmol) was added to the mixture. The reaction was heated at 60 °C and stirred for 48 h. The PCL precursor was grafted to the resin. The catalyst and resin were removed after passing through neutral alumina. Other copolymers ($\text{PEG}_{113}\text{-SS-PCL}_{22}$, $\text{PEG}_{113}\text{-SS-PCL}_{61}$) with different molar masses of PCL were synthesized through the same procedure.

Characterization. ¹H NMR. The ¹H NMR spectra were recorded on a Bruker AV400 spectrometer operating at 400 MHz. Each sample was dissolved in deuterated chloroform (CDCl_3 , 0.6 mL) and tetramethylsilane (TMS) was used as an internal standard.

Gel Permeation Chromatography (GPC). The weight-average molar mass (M_w), number-average molar mass (M_n), and the polydispersity index ($\text{PDI} = M_w/M_n$) of the samples were determined by a Waters 1515 gel permeation chromatography (GPC) instrument equipped with three Waters Styragel columns (HR2, HR4, and HR6) and connected with a refractive index detector (RI, Wyatt WREX-02) at 35 °C. THF was used as the eluent at a flow of 1.0 mL/min, and the instrument was calibrated by a series of polystyrene standards.

Preparation of PEG-R-PCL Micelles Loaded with Dyes. PEG-SS-PCL diblock copolymer (10.0 mg), DiO (0.075 mg), and DiI (0.075 mg) were dissolved in acetone (0.50 mL). The solution was dropped into Milli-Q ultrapure water (5.00 mL) at a speed of 2.8 mL/h. Because acetone is miscible with water and PCL is insoluble in water, PEG-SS-PCL micelles were formed. Subsequently, the micellar solution was dialyzed against 1 L Milli-Q ultrapure water with a dialysis bag (Green Bird, molecular weight cutoff (MWCO) = 14 000

Da) for 48 h. The water was changed after 24 h. The free PEG was removed during the dialysis procedure. The polymer concentration after dialysis was measured after vacuum drying the solution. The preparation of PEG-CC-PCL micelles is similar.

Determination of Critical Micelle Concentration (CMC) of PEG-R-PCL. The CMC values of PEG-R-PCL were determined using pyrene as a fluorescence probe on an F-4600 fluorescence spectrophotometer (Hitachi High-Technologies Corporation, Tokyo Japan).⁶⁵ The excitation spectra were recorded by scanning the excitation wavelength from 280 to 380 nm at a fixed emission wavelength of 390 nm. The widths of both excitation and emission slits were set at 2.5 nm, and the PMT voltage was 900 V. The intensity (peak height) ratio of I_{338}/I_{335} from the excitation spectra was analyzed as a function of the copolymer concentration. The CMC value was calculated from the intersection between two lines obtained by fitting the points at the inflection and at low concentrations.

Sizes and Aggregation Kinetics of PEG-R-PCL Micelles. The average hydrodynamic radii of micelles were determined by dynamic light scattering (DLS). Measurements were carried out at 20 °C by a commercial Laser Light Scattering spectrometer (ALV/CGS-8F S/N 028, Germany) with a 22 mW UNIPHASE He-Ne laser ($\lambda = 632.8$ nm) as the light source. The micellar solutions were filtered through a 450 nm hydrophilic PTFE filter (Millipore, Bedford, MA) to remove dust before measurements. For the measurements of aggregation kinetics of different PEG-SS-PCL micelles in response to 10 mM DTT aqueous solutions, after degassing with nitrogen for 2 min, the concentrated DTT aqueous solution was filtered through a 450 nm hydrophilic PTFE filter. The DTT aqueous solution and PEG-SS-PCL micellar solutions were mixed. The final solution contains 1.0 mg/mL of PEG-SS-PCL micelles and 10 mM of DTT. The average hydrodynamic radius and the hydrodynamic radius distribution were determined using DLS with a duration of 5 min and a scattering angle of 30°.

Guest Exchange Dynamics of PEG-SS-PCL Micelles. Two aqueous solutions containing PEG-SS-PCL micelles loaded with 0.75 wt % DiI or 0.75 wt % DiO were prepared separately. After degassing with nitrogen for 2 min, the concentrated DTT aqueous solution was filtered through a 450 nm hydrophilic PTFE filter. The DTT aqueous solution and two micellar solutions filtered through a 450 nm hydrophilic PTFE filter were mixed. The final concentrations of copolymer and DTT were 1.0 mg/mL and 10 mM, respectively. The fluorescence spectroscopy was recorded on an F-4600 fluorescence spectrophotometer (Hitachi High-Technologies Corporation, Tokyo Japan). The emission spectra were obtained by scanning the emission wavelength from 490 to 600 nm at a fixed excitation wavelength of 488 nm. The widths of both excitation and emission slits were set at 2.5 nm, and the PMT voltage was 950 V.

Flow Cytometry Analysis. For flow cytometric analysis, HeLa cells were seeded at a density of 2×10^5 cells per well in 6-well plates in 1.5 mL of a medium at 37 °C in a 5% CO_2 humidified atmosphere. The original media were replaced with media with different micelles loaded with DiO, where the final concentration of DiO was 7.5 $\mu\text{g/mL}$. The cells were incubated for different times at 37 °C and then rinsed with PBS. The cells were trypsinized and resuspended in cold PBS (0.5 mL) for flow cytometric analysis at the FL1-channel using a BD FACS

Calibur flow cytometer. For each sample, 10 000 events were collected. Cells without any treatment were set as control.

FRET Imaging. FRET imaging was performed on an Olympus IX81 inverted-microscope. FRET images were acquired with 488 nm excitation and spectral filters of 488–524 nm and 561–605 nm for the detection of fluorescent emission of DiO and DiI, respectively. HeLa cells were seeded at a density of 80 000 cells per well in 35 mm glass bottom cell culture dish in 1.5 mL of a medium at 37 °C in a 5% CO₂ humidified atmosphere. The original media were replaced with media with different micelles loaded with both DiO and DiI, where the final concentrations of DiO and DiI were 7.5 μg/mL. And then, the dishes were placed in the CO₂ incubator. The images were collected every 10 min for 3 h.

RESULTS AND DISCUSSION

Synthesis of PEG-R-PCL Copolymers. As shown in Scheme 1, PEG–SS–PCL was synthesized by a Cu-catalyzed azide–alkyne cycloaddition (click chemistry) of PEG₁₁₃–N₃ and ≡–SS–PCL_{*n*}. First, PEG₁₁₃–OTs was prepared through the reaction between PEG₁₁₃–OH and *p*-benzenesulfonyl chloride using TEA as a catalyst in DCM, and the ¹H NMR spectrum of PEG₁₁₃–OTs is shown in Figure S1. Then azidation substitution reaction by sodium azide in DMF led to PEG₁₁₃–N₃, and Figure S2 shows the ¹H NMR spectrum of PEG₁₁₃–N₃, indicating the high azidation efficiency (~98%). On the other hand, ≡–R–PCL_{*n*} were synthesized through ring-opening polymerization of ε-caprolactone using ≡–SS–OH or ≡–CC–OH as initiators and Sn(EH)₂ as a catalyst in toluene. The ¹H NMR spectra of the initiators ≡–SS–OH and ≡–CC–OH are shown in Figures S3 and S4, indicating high purity of the samples. The molecular weight of PCL was controlled by the ratio of the monomer to the initiator. A typical ¹H NMR spectrum of ≡–SS–PCL₃₉ is shown in Figure S5. The azide–alkyne cycloaddition of PEG₁₁₃–N₃ and ≡–SS–PCL_{*n*} catalyzed by CuBr was carried out in DMF at 50 °C for 48 h. Figure 1

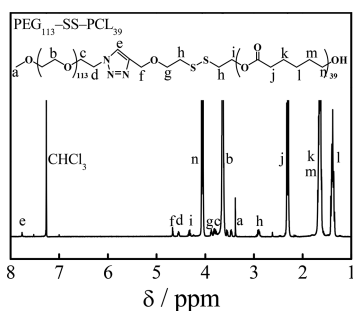


Figure 1. ¹H NMR spectrum of PEG₁₁₃–SS–PCL₃₉ in CDCl₃, where the copolymer concentration was ~15 mg/mL.

shows a typical ¹H NMR spectrum of the copolymer PEG₁₁₃–SS–PCL₃₉ with 39 denoting the number of CL repeating units per copolymer chain calculated from the integral area of the peaks (j–n). The integral area ratio of a characteristic peak (e) belonging to “click” ring verifies high reaction efficiency (~93%). The ¹H NMR spectra of two other block copolymers (PEG₁₁₃–SS–PCL₂₂ and PEG₁₁₃–SS–PCL₆₁) are shown in Figures S6 and S7. As shown in Figure 2, GPC curves of PEG₁₁₃–N₃, ≡–SS–PCL₃₉, and PEG₁₁₃–SS–PCL₃₉ show unimodal distributions with low PDI values for all three polymers and the peak of copolymer PEG₁₁₃–SS–PCL₃₉ shifts to a shorter retention time compared with that of PEG₁₁₃–N₃

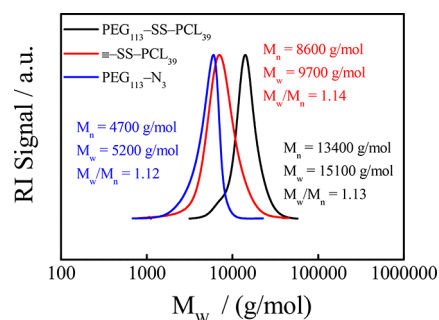


Figure 2. GPC curves of PEG₁₁₃–SS–PCL₃₉, ≡–SS–PCL₃₉, and PEG₁₁₃–N₃. The copolymer concentrations were ~5 mg/mL. Temperature: 35 °C. Eluent: THF at a flow rate of 1.0 mL/min. Standards: narrowly distributed polystyrenes.

and ≡–SS–PCL₃₉, indicating the complete coupling of PEG₁₁₃–N₃ and ≡–SS–PCL₃₉. The GPC curves of the two other copolymers (PEG₁₁₃–SS–PCL₂₂ and PEG₁₁₃–SS–PCL₆₁) are shown in Figure S8. The GPC and ¹H NMR characterization results of all the copolymers are summarized in Table 1.

Micelle Formation and Characterization. The critical micelle concentrations (CMC) of amphiphilic copolymers with different molar masses were determined using pyrene as a fluorescence probe. As shown in Figure 3, the CMC of PEG₁₁₃–SS–PCL₃₉ obtained from the intersection between the fitted line of the points at low concentrations is 3.91×10^{-3} mg/mL and the CMC of PEG₁₁₃–SS–PCL₂₂ and PEG₁₁₃–SS–PCL₆₁ are 6.69×10^{-3} mg/mL and 2.54×10^{-3} mg/mL, respectively, as shown in Figure S9. Note that the CMC values of PEG–SS–PCL decrease gradually with the increase in the molar mass of the hydrophobic PCL block when the chain length of PEG hydrophilic chain is kept as the same, which is consistent with other reports.^{66,67}

PEG–SS–PCL micelles were prepared by adding an acetone solution containing PEG–SS–PCL block copolymers and two dyes (DiO and DiI) into the ultrapure water at a speed of 2.8 mL/h using a PHD 2000 syringe pump. The average hydrodynamic radius ($\langle R_h \rangle$) and hydrodynamic radius distributions ($f(R_h)$) of the formed micelles by DLS are shown in Figure 4. The results indicate that the $\langle R_h \rangle$ s of PEG–SS–PCL micelles are in the regime of 50–80 nm and the PDI values are below 0.30, indicating a narrow distribution of the micelles. Moreover, $\langle R_h \rangle$ of the micelles increases with the molar mass of the hydrophobic PCL block. The surface density of PEG of the micelles was determined according to the approach as described in our previous work.⁶⁸ For example, a typical Zimm plot in Figure S10 shows that the M_w of PEG₁₁₃–SS–PCL₃₉ micelles is 6.57×10^7 g/mol and the estimated surface density of PEG of the PEG₁₁₃–SS–PCL₃₉ micelles is ~1.14 chain/nm². The characterization results of CMC, $\langle R_h \rangle$, PDI and the surface density of PEG of these micelles formed by PEG₁₁₃–SS–PCL₂₂, PEG₁₁₃–SS–PCL₃₉, and PEG₁₁₃–SS–PCL₆₁ are also summarized in Table 1. Note that the surface density of PEG decreases slightly with the increase in PCL length.

The pair of two dyes (DiO and DiI) is widely used in various FRET experiments. The energy transfer is efficient when the average distance between the donor DiO and the acceptor DiI is less than 2–10 nm and the Förster radius, the characteristic distance with 50% energy transfer efficiency, is 4.5 nm for this

Table 1. Characterization Results of the Block Copolymers and the Micelles

samples	copolymers				micelles			
	¹ H NMR		GPC		DLS		CMC (mg/L)	σ (chain/nm ²)
	M_n (g/mol)	M_n (g/mol)	M_w (g/mol)	M_w/M_n	$\langle R_h \rangle$ (nm)	PDI		
PEG ₁₁₃ -SS-PCL ₂₂	7700	10100	11200	1.10	51.3	0.24	6.69	1.21
PEG ₁₁₃ -SS-PCL ₃₉	9600	13400	15100	1.13	61.8	0.26	3.91	1.14
PEG ₁₁₃ -SS-PCL ₆₁	12100	16600	19200	1.16	82.9	0.26	2.54	1.10

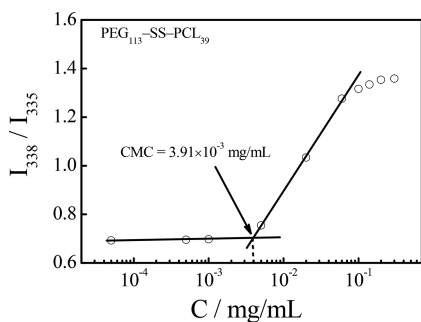


Figure 3. Plot of the fluorescence intensity ratio I_{338}/I_{335} obtained from excitation spectra of pyrene as a function of the PEG₁₁₃-SS-PCL₃₉ copolymer concentrations. The excitation spectrum was obtained by scanning from 280 to 380 nm at a fixed emission wavelength of 390 nm. The widths of both excitation and emission slits were set at 2.5 nm and the PMT voltage was 900 V.

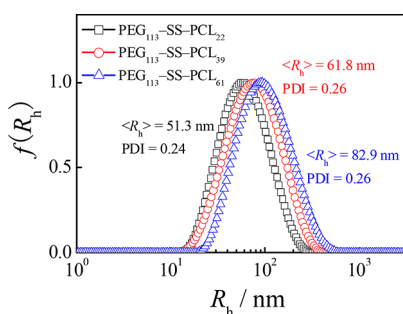


Figure 4. Hydrodynamic radius distribution $f(R_h)$ of PEG₁₁₃-SS-PCL₂₂ (\square), PEG₁₁₃-SS-PCL₃₉ (red \circ), and PEG₁₁₃-SS-PCL₆₁ (blue \triangle) micelles loaded with 0.75 wt % DiI and 0.75 wt % DiO formed in aqueous solutions, where the copolymer concentrations were 1.0 mg/mL.

FRET pair.^{69,70} In our experiments, when both DiO and DiI molecules were loaded into the micelles, the fluorescence resonance energy transfer (FRET) ratio defined as $\gamma_{\text{FRET}} = I_{\text{DiI}} / (I_{\text{DiO}} + I_{\text{DiI}})$ is 0.88, which is calculated from fluorescence emission spectra of PEG₁₁₃-SS-PCL₃₉ micelles aqueous solution shown in Figure S11, where I_{DiO} and I_{DiI} were the fluorescence intensity of the peaks at 510 and 573 nm, respectively. When the copolymer micelles loaded with the dyes were dissolved in acetone which is a good solvent for the two blocks (PEG and PCL) and the dyes, micelles dissociated into diblock copolymers and the FRET ratio decreases to 0.19 due to the increase in the average distance between DiO and DiI molecules, which is in accordance with the results obtained by Cheng et al.⁴² So the stability of micelles and the release kinetics of the dyes could be studied by monitoring the change of the FRET ratio.

Aggregation Kinetics of PEG-SS-PCL Micelles. The cleavage of the single disulfide bond between PEG and PCL blocks with the addition of DTT aqueous solution can lead to

the aggregation of the micelles.¹³ The aggregation kinetics of different PEG-SS-PCL micelles in response to 10 mM DTT was studied by dynamic light scattering (DLS), as shown in Figure 5. With the addition of DTT, the average hydrodynamic

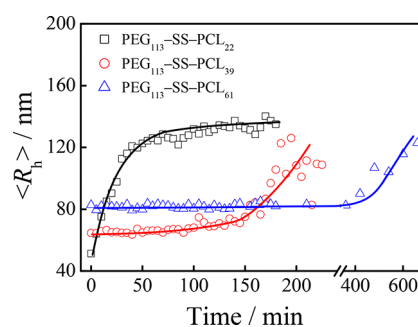


Figure 5. Time dependence of average hydrodynamic radius of PEG₁₁₃-SS-PCL₂₂ (\square), PEG₁₁₃-SS-PCL₃₉ (red \circ), and PEG₁₁₃-SS-PCL₆₁ (blue \triangle) micelles loaded with 0.75 wt % DiI and 0.75 wt % DiO in aqueous solutions containing 10 mM DTT, where the copolymer concentrations were 1.0 mg/mL.

radius ($\langle R_h \rangle$) of PEG₁₁₃-SS-PCL₂₂ micelles increases from 50 to 125 nm within 100 min and then levels off after about 120 min. The time dependence of $\langle R_h \rangle$ of PEG₁₁₃-SS-PCL₃₉ micelles can be well fitted by an equation $\langle R_h \rangle = 54t^{0.19}$, indicating a diffusion-limited cluster-cluster aggregation (DLCA).^{71,72} However, the aggregation kinetics of PEG₁₁₃-SS-PCL₃₉ and PEG₁₁₃-SS-PCL₆₁ micelles are similar to each other, but different from that of PEG₁₁₃-SS-PCL₂₂ micelles. Figure 5 shows that the $\langle R_h \rangle$ of PEG₁₁₃-SS-PCL₃₉ micelles only slightly increases in ~ 150 min and then increases to 120 nm within 200 min. PEG₁₁₃-SS-PCL₆₁ micelles have a similar aggregation process but a longer induction period of ~ 400 min. The aggregation process can be well fitted by an exponential function, that is, $\langle R_h \rangle = 57 + 4e^{t/86}$ for PEG₁₁₃-SS-PCL₃₉ micelles and $\langle R_h \rangle = 79 + e^{t/183}$ for PEG₁₁₃-SS-PCL₆₁ micelles, indicating a reaction-limited cluster-cluster aggregation (RLCA).⁷³ The M_w s of PEG-SS-PCL micelles measured by LLS are 2.06×10^7 g/mol, 6.57×10^7 g/mol, and 1.85×10^8 g/mol for PEG₁₁₃-SS-PCL₂₂, PEG₁₁₃-SS-PCL₃₉, and PEG₁₁₃-SS-PCL₆₁, respectively. Thus, the average number density of the micelles formed by PEG₁₁₃-SS-PCL₂₂, PEG₁₁₃-SS-PCL₃₉, and PEG₁₁₃-SS-PCL₆₁ are 2.93×10^{13} mL⁻¹, 9.15×10^{12} mL⁻¹, and 2.72×10^{12} mL⁻¹, respectively, which follows the order: PEG₁₁₃-SS-PCL₂₂ > PEG₁₁₃-SS-PCL₃₉ > PEG₁₁₃-SS-PCL₆₁. So the difference in aggregation processes might be due to the difference in the average number density of these micelles, that is, the higher average number density may result in a faster aggregation rate of PEG-SS-PCL micelles.

Guest Exchange Dynamics of PEG-SS-PCL Micelles.

Figure 6a shows the time-resolved fluorescence emission spectra of PEG₁₁₃-SS-PCL₃₉ micelles in aqueous solutions without the addition of DTT when two micelles loaded with

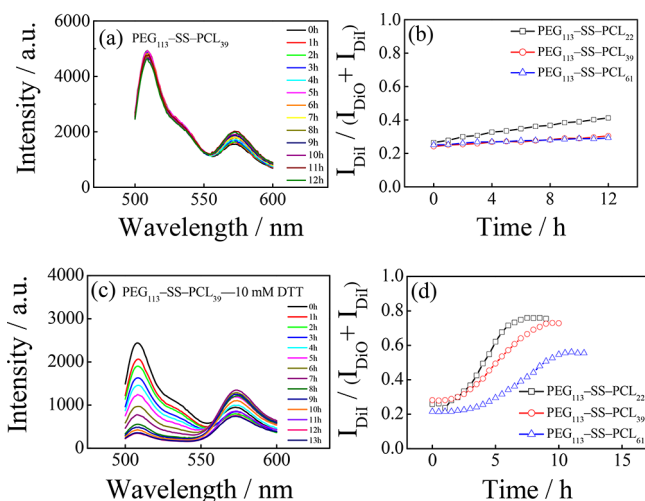


Figure 6. (a,c) Time-resolved fluorescence emission spectra of PEG₁₁₃-SS-PCL₃₉ micelles loaded with 0.75 wt % DiI or 0.75 wt % DiO separately in aqueous solutions without the addition of DTT (a) and with the addition of 10 mM DTT (c). The emission spectrum was obtained by scanning the emission wavelength from 490 to 600 nm at a fixed excitation wavelength of 488 nm. The widths of both excitation and emission slits were set at 2.5 nm and the PMT voltage was 950 V. (b,d) Time traces of FRET ratios ($\gamma_{\text{FRET}} = I_{\text{DiI}} / (I_{\text{DiO}} + I_{\text{DiI}})$) of PEG₁₁₃-SS-PCL₂₂ (□), PEG₁₁₃-SS-PCL₃₉ (red ○), and PEG₁₁₃-SS-PCL₆₁ (blue △) in aqueous solutions without the addition of DTT (b) and with the addition of 10 mM DTT (d), where the copolymer concentrations were 1.0 mg/mL.

DiO and DiI molecules separately were mixed. The fluorescence intensity of the donor DiO (I_{DiO}) at 510 nm is strong, and that of the acceptor DiI (I_{DiI}) at 573 nm is weak, indicating the lower FRET ratio (0.24) as DiO and DiI molecules are in different micelles. Then I_{DiO} slightly decreases and I_{DiI} increases with time, indicating that the dye molecules escape from the original micelles into other micelles during the exchange of the diblock copolymer chains between micelles. The diffusion induced guest exchange is the main pathway because of the intact PEG shell of the micelles. Both PEG₁₁₃-SS-PCL₂₂ and PEG₁₁₃-SS-PCL₆₁ micelles exhibit similar phenomena, as shown in Figure S12. Figure 6b shows the time dependence of $I_{\text{DiI}} / (I_{\text{DiO}} + I_{\text{DiI}})$ of the three different micelles. All of the FRET ratios increase slightly with time and in detail, the FRET ratio increases from 0.26 to 0.41, from 0.24 to 0.30, and from 0.25 to 0.29 within 12 h for PEG₁₁₃-SS-PCL₂₂, PEG₁₁₃-SS-PCL₃₉, and PEG₁₁₃-SS-PCL₆₁ micelles, respectively. The increase rate of the FRET ratio of PEG₁₁₃-SS-PCL₂₂ micelles is the highest, presumably due to the lowest encapsulation stability because of the highest chain exchange rate of the PEG₁₁₃-SS-PCL₂₂ micelles with the shortest core chain length. Choi et al. suggested that chain exchange in micelles formed by poly(styrene-*b*-ethylene-*alt*-propylene) (PS-PEP) was facilitated by reducing the chain length of the hydrophobic PS block using time-resolved small-angle neutron scattering,⁷⁴ which is consistent with our results.

When DiI-loaded and DiO-loaded PEG₁₁₃-SS-PCL₃₉ micelles were mixed in aqueous solutions containing 10 mM DTT, the change of the fluorescence emission spectra with time is different from that without the addition of DTT. As shown in Figure 6c, I_{DiO} decreases dramatically, and I_{DiI} increases with time, indicating the increase in the exchange rate of the dyes between different micelles due to the cleavage

of the PEG chains. The time-resolved fluorescence emission spectra of two other micelles (PEG₁₁₃-SS-PCL₂₂ and PEG₁₁₃-SS-PCL₆₁ micelles) are similar to that of PEG₁₁₃-SS-PCL₃₉ micelles at the beginning of the experiments, as shown in Figure S13. For PEG₁₁₃-SS-PCL₃₉ micelles, after 8 h the decrease in the fluorescent intensity of both DiI and DiO is due to the precipitation of unstable large aggregates, as shown in Figure S14. The time dependence of the FRET ratios of three different micelles in aqueous solutions containing 10 mM DTT is summarized in Figure 6d. For PEG₁₁₃-SS-PCL₃₉ micelles with the addition of DTT, the FRET ratio increases much faster from 0.26 to 0.74 in 8 h. Dye exchange rate of the micelles in aqueous solutions containing 10 mM DTT follows the order: PEG₁₁₃-SS-PCL₂₂ > PEG₁₁₃-SS-PCL₃₉ > PEG₁₁₃-SS-PCL₆₁, indicating that detachment of PEG shells increases collision-induced dye exchange rate, and PEG₁₁₃-SS-PCL₂₂ exhibited the fastest dye exchange rate because of the highest average number and smallest hydrodynamic radius of the PEG₁₁₃-SS-PCL₂₂ micelles. Note that the detachment of PEG shells also increases the efficiency of the diffusion-induced dye exchange rate because now the dyes can easily diffuse into the aqueous solution without PEG shell as a barrier. Comparing with the aggregation kinetics of micelles shown in Figure 5, the increase rates of FRET ratios are slower than that of $\langle R_h \rangle$ s for all three kinds of micelles, indicating that the exchange of dyes (DiI and DiO) between the aggregated micelles is not instantaneous and needs time.

Internalization of PEG-SS-PCL Micelles in Vitro. The internalization of the micelles formed by PEG₁₁₃-CC-PCL₄₁ and PEG₁₁₃-SS-PCL₃₉ was studied. The flow cytometric analyses of HeLa cells incubated with DiO-loaded PEG₁₁₃-CC-PCL₄₁ or DiO-loaded PEG₁₁₃-SS-PCL₃₉ micelles for 2 h and the mean fluorescence intensities (MFI) of cells incubated with DiO-loaded PEG₁₁₃-CC-PCL₄₁ or PEG₁₁₃-SS-PCL₃₉ micelles after indicated times are summarized in Figure S15. The result shows that fluorescence peak of HeLa cells incubated with the micelles formed by PEG₁₁₃-SS-PCL₃₉ exhibits right shift relative to HeLa cells incubated with PEG₁₁₃-CC-PCL₄₁ micelles, implying that reduction-responsive micelles have higher intracellular delivery as compared to the PEG₁₁₃-CC-PCL₄₁ micelles, which is consistent with the reported findings.^{13,21}

The effect of hydrophobic PCL chain length of reduction-responsive micelles loaded with DiO on the cellular uptake behavior was investigated using flow cytometric analyses. As shown in Figure 7, the result indicates that the DiO fluorescence intensity increases with the incubation time within

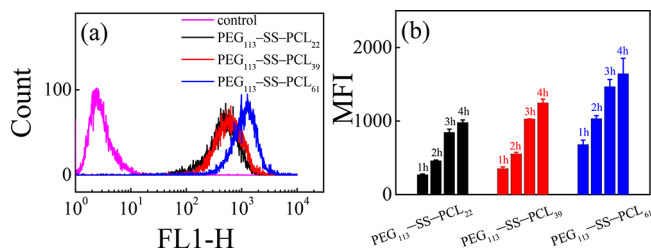


Figure 7. (a) Flow cytometric analyses of HeLa cells after 2 h incubation with different DiO-loaded PEG-SS-PCL micelles. (b) The mean fluorescence intensities (MFI) of cells incubated with DiO-loaded PEG-SS-PCL micelles after indicated times. Flow cytometric analysis at the FL1-channel and 10 000 events were collected for each sample. Cells without any treatment were set as control.

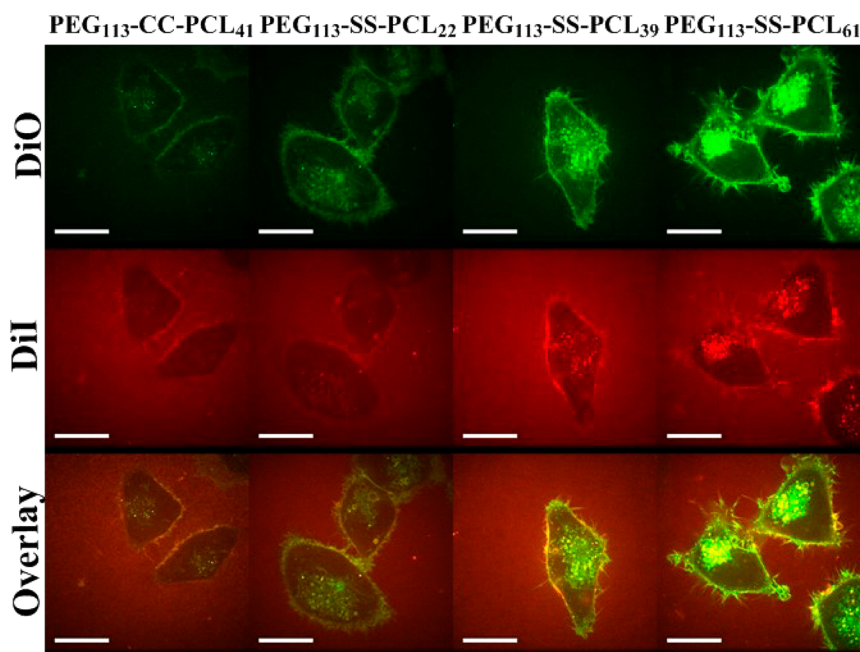


Figure 8. Confocal microscopy images of HeLa cell incubation with PEG₁₁₃-CC-PCL₄₁, PEG₁₁₃-SS-PCL₂₂, PEG₁₁₃-SS-PCL₃₉, and PEG₁₁₃-SS-PCL₆₁ micelles loaded with both 0.75 wt % DiI and 0.75 wt % DiO for 2 h. FRET images were acquired with 488 nm excitation and spectral filters of 488–524 nm and 561–605 nm. Within each image set, green color is the image of DiO's emission shown in the top line, and red color is the image of DiI's emission shown in the middle line. Yellow color is overlay of green and red shown in the bottom line. Scale bar is 10 μ m.

4 h. Moreover, cells treated with PEG₁₁₃-SS-PCL₆₁ micelles exhibit the highest fluorescence intensity. The fluorescence intensity increases with the PCL chain length, presumably because the increase in PCL chain length led to the relatively larger hydrodynamic radius of PEG-SS-PCL micelles as the surface PEG density only slightly decreases, as shown in Table 1. Our finding is consistent with the results reported by Win and Feng, who stated that the uptake of poly(lactic-co-glycolic acid) (PLGA) nanoparticles coated with poly(vinyl alcohol) (PVA) with a diameter of 100 nm is 2.3-fold greater than that of 50 nm nanoparticles.⁷⁵

Four kinds of micelles loaded with both DiO and DiI formed by PEG₁₁₃-CC-PCL₄₁, PEG₁₁₃-SS-PCL₂₁, PEG₁₁₃-SS-PCL₃₉, and PEG₁₁₃-SS-PCL₄₄ were added into the cell culture medium, and the cellular internalization behavior of PEG-R-PCL micelles in vitro was monitored using a confocal fluorescence microscopy. Figure 8 shows confocal microscopy images of HeLa cells after 2 h incubation and these FRET images were acquired with 488 nm excitation and spectral filters of 488–524 nm and 561–605 nm for the detection of fluorescent emission of DiO and DiI, respectively. HeLa cells treated with reduction-responsive micelles exhibit higher fluorescence intensity than those treated with the PEG-CC-PCL micelles, which is in agreement with our results of flow cytometric analyses and the reported findings.⁵⁰ It is also clear that the green (DiO) and red (DiI) fluorescence intensities increase with the PCL chain lengths. The strong red fluorescence intensity in the extracellular space for both reduction-nonresponsive and reduction-responsive micelles indicates a high energy transfer from the donor molecules (DiO) to the acceptor molecules (DiI) because they are nearby and the micelles are stable during the incubation. Note that the FRET ratio outside the HeLa cells is ~ 0.85 and the fluorescence intensity in the extracellular space for all the micelles is similar because the amount of micelles is excessive in our study. The

red fluorescence signal (DiI) located on the cell membrane and in the cell interior suggests that some whole micelles internalize into cells. However, we cannot exclude the possibility that some DiI dyes released from micelles locate in the proximate position close to those released DiO dyes as some groups also observed the recovery of FRET efficacy due to the colocalization of FRET dyes after internalization.^{50,51} For PEG₁₁₃-SS-PCL₃₉ micelles, a green color is observed on the cell membrane and the intracellular space and the average FRET ratios on the cell membrane and in the intracellular space reduce to ~ 0.59 and ~ 0.52 in 120 min, respectively. Figure S16 shows the time traces of DiO and DiI average fluorescence intensities on the cell membrane, in the cell exterior, and the cell interior. The average FRET ratios calculated from fluorescence intensities of DiO and DiI on the membrane and in the intracellular space decrease from 0.73 to 0.56 and from 0.74 to 0.49 in 180 min, respectively, as shown in Figure 9, suggesting that the micelles could enter into the HeLa cells once they are added to the medium, and then the guests loaded in micelles start to release immediately.

CONCLUSIONS

In summary, we have successfully synthesized disulfide-linked copolymer PEG-SS-PCL with the same chain length of hydrophilic block PEG but different chain lengths of hydrophobic block PCL by the use of ring-opening polymerization and click chemistry. Longer PCL chains lead to lower CMC values and larger average hydrodynamic radius of micelles. The aggregation rates of PEG-SS-PCL micelles in response to 10 mM DTT observed by DLS follow the order: PEG₁₁₃-SS-PCL₂₂ > PEG₁₁₃-SS-PCL₃₉ > PEG₁₁₃-SS-PCL₆₁. The guest exchange of PEG-SS-PCL micelles in response to 10 mM DTT was studied using the FRET method. The results suggest that longer hydrophobic chains lead to slower guest exchange rates. Moreover, the internalization of PEG-SS-PCL micelles

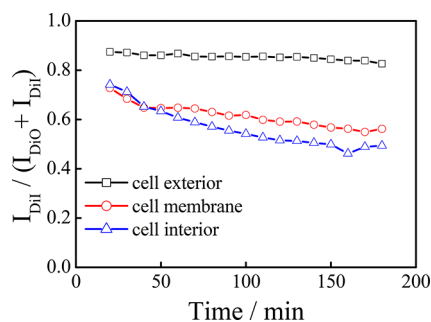


Figure 9. Time traces of FRET ratios at cell membrane, cell exterior, and cell interior calculated from confocal microscopy images of HeLa cells incubated with 0.2 mg/mL PEG₁₁₃-SS-PCL₃₉ micelles loaded with both 0.75 wt % DiI and 0.75 wt % DiO.

in vitro measured by flow cytometric analysis and confocal fluorescence microscopy show that micelles with longer hydrophobic chains exhibit higher cellular internalization, implying that higher cell uptake could compensate the slower guest release rate.

■ ASSOCIATED CONTENT

Supporting Information

The Supporting Information is available free of charge on the ACS Publications website at DOI: 10.1021/acs.jpcc.7b06165.

¹H NMR spectra; GPC curves; fluorescence intensity ratio I_{338}/I_{335} ; Zimm plot; fluorescence emission spectra; flow cytometric analyses (PDF)

■ AUTHOR INFORMATION

Corresponding Author

*E-mail: xdye@ustc.edu.cn. Telephone: 86-551-63606742.

ORCID

Xiaodong Ye: 0000-0003-2143-1726

Notes

The authors declare no competing financial interest.

■ ACKNOWLEDGMENTS

The authors thank Professor Jun Wang and Professor Yucai Wang for generously providing access to the flow cytometry. The financial support of the National Natural Scientific Foundation of China (NNSFC) Projects (21674107 and 21274140) and the Fundamental Research Funds for the Central Universities (WK2340000066) is gratefully acknowledged.

■ REFERENCES

- (1) Tanner, P.; Baumann, P.; Enea, R.; Onaca, O.; Palivan, C.; Meier, W. Polymeric Vesicles: from Drug Carriers to Nanoreactors and Artificial Organelles. *Acc. Chem. Res.* **2011**, *44*, 1039–1049.
- (2) Prabhu, R. H.; Patravale, V. B.; Joshi, M. D. Polymeric Nanoparticles for Targeted Treatment in Oncology: Current Insights. *Int. J. Nanomed.* **2015**, *10*, 1001–1018.
- (3) Hubbell, J. A.; Chilkoti, A. Nanomaterials for Drug Delivery. *Science* **2012**, *337*, 303–305.
- (4) Bourzac, K. Nanotechnology Carrying Drugs. *Nature* **2012**, *491*, S58–S60.
- (5) Cabral, H.; Kataoka, K. Progress of Drug-Loaded Polymeric Micelles into Clinical Studies. *J. Controlled Release* **2014**, *190*, 465–476.

(6) Wilhelm, S.; Tavares, A. J.; Dai, Q.; Ohta, S.; Audet, J.; Dvorak, H. F.; Chan, W. C. W. Analysis of Nanoparticle Delivery to Tumours. *Nat. Rev. Mater.* **2016**, *1*, 16014.

(7) Nakamura, Y.; Mochida, A.; Choyke, P. L.; Kobayashi, H. Nanodrug Delivery: Is the Enhanced Permeability and Retention Effect Sufficient for Curing Cancer? *Bioconjugate Chem.* **2016**, *27*, 2225–2238.

(8) Zhang, Q.; Ko, N. R.; Oh, J. K. Recent Advances in Stimuli-Responsive Degradable Block Copolymer Micelles: Synthesis and Controlled Drug Delivery Applications. *Chem. Commun.* **2012**, *48*, 7542–7552.

(9) Mura, S.; Nicolas, J.; Couvreur, P. Stimuli-Responsive Nano-carriers for Drug Delivery. *Nat. Mater.* **2013**, *12*, 991–1003.

(10) Torchilin, V. P. Multifunctional, Stimuli-Sensitive Nanoparticulate Systems for Drug Delivery. *Nat. Rev. Drug Discovery* **2014**, *13*, 813–827.

(11) Blum, A. P.; Kammeyer, J. K.; Rush, A. M.; Callmann, C. E.; Hahn, M. E.; Gianneschi, N. C. Stimuli-Responsive Nanomaterials for Biomedical Applications. *J. Am. Chem. Soc.* **2015**, *137*, 2140–2154.

(12) Meng, F. H.; Hennink, W. E.; Zhong, Z. Y. Reduction-Sensitive Polymers and Bioconjugates for Biomedical Applications. *Biomaterials* **2009**, *30*, 2180–2198.

(13) Sun, H. L.; Guo, B. N.; Cheng, R.; Meng, F. H.; Liu, H. Y.; Zhong, Z. Y. Biodegradable Micelles with Sheddable Poly(ethylene glycol) Shells for Triggered Intracellular Release of Doxorubicin. *Biomaterials* **2009**, *30*, 6358–6366.

(14) Sun, H. L.; Guo, B. N.; Li, X. Q.; Cheng, R.; Meng, F. H.; Liu, H. Y.; Zhong, Z. Y. Shell-Sheddable Micelles Based on Dextran-SS-Poly(ϵ -caprolactone) Diblock Copolymer for Efficient Intracellular Release of Doxorubicin. *Biomacromolecules* **2010**, *11*, 848–854.

(15) Wang, W.; Sun, H. L.; Meng, F. H.; Ma, S. B.; Liu, H. Y.; Zhong, Z. Y. Precise Control of Intracellular Drug Release and Anti-Tumor Activity of Biodegradable Micellar Drugs via Reduction-Sensitive Shell-Shedding. *Soft Matter* **2012**, *8*, 3949–3956.

(16) Chen, W.; Zou, Y.; Jia, J. N.; Meng, F. H.; Cheng, R.; Deng, C.; Feijen, J.; Zhong, Z. Y. Functional poly(ϵ -caprolactone)s via Copolymerization of ϵ -Caprolactone and Pyridyl Disulfide-Containing Cyclic Carbonate: Controlled Synthesis and Facile Access to Reduction-Sensitive Biodegradable Graft Copolymer Micelles. *Macromolecules* **2013**, *46*, 699–707.

(17) Chen, W.; Zhong, P.; Meng, F. H.; Cheng, R.; Deng, C.; Feijen, J.; Zhong, Z. Y. Redox and pH-Responsive Degradable Micelles for Dually Activated Intracellular Anticancer Drug Release. *J. Controlled Release* **2013**, *169*, 171–179.

(18) Zhong, Y. N.; Yang, W. J.; Sun, H. L.; Cheng, R.; Meng, F. H.; Deng, C.; Zhong, Z. Y. Ligand-Directed Reduction-Sensitive Shell-Sheddable Biodegradable Micelles Actively Deliver Doxorubicin into the Nuclei of Target Cancer Cells. *Biomacromolecules* **2013**, *14*, 3723–3730.

(19) Lv, J. L.; Sun, H. L.; Zou, Y.; Meng, F. H.; Dias, A. A.; Hendriks, M.; Feijen, J.; Zhong, Z. Y. Reductively Degradable α -Amino Acid-based Poly(ester amide)-graft-galactose Copolymers: Facile Synthesis, Self-Assembly, and Hepatoma-Targeting Doxorubicin Delivery. *Biomater. Sci.* **2015**, *3*, 1134–1146.

(20) Zhu, Y. Q.; Zhang, J.; Meng, F. H.; Deng, C.; Cheng, R.; Feijen, J.; Zhong, Z. Y. cRGD-Functionalized Reduction-Sensitive Shell-Sheddable Biodegradable Micelles Mediate Enhanced Doxorubicin Delivery to Human Glioma Xenografts in Vivo. *J. Controlled Release* **2016**, *233*, 29–38.

(21) Tang, L. Y.; Wang, Y. C.; Li, Y.; Du, J. Z.; Wang, J. Shell-Detachable Micelles Based on Disulfide-Linked Block Copolymer As Potential Carrier for Intracellular Drug Delivery. *Bioconjugate Chem.* **2009**, *20*, 1095–1099.

(22) Khorsand Sourkahi, B.; Cunningham, A.; Zhang, Q.; Oh, J. K. Biodegradable Block Copolymer Micelles with Thiol-Responsive Sheddable Coronas. *Biomacromolecules* **2011**, *12*, 3819–3825.

(23) Cunningham, A.; Ko, N. R.; Oh, J. K. Synthesis and Reduction-Responsive Disassembly of PLA-based Mono-Cleavable Micelles. *Colloids Surf., B* **2014**, *122*, 693–700.

- (24) Ko, N. R.; Oh, J. K. Glutathione-Triggered Disassembly of Dual Disulfide Located Degradable Nanocarriers of Polylactide-Based Block Copolymers for Rapid Drug Release. *Biomacromolecules* **2014**, *15*, 3180–3189.
- (25) Klaiherd, A.; Nagamani, C.; Thayumanavan, S. Multi-Stimuli Sensitive Amphiphilic Block Copolymer Assemblies. *J. Am. Chem. Soc.* **2009**, *131*, 4830–4838.
- (26) Jiwanich, S.; Ryu, J. H.; Bickerton, S.; Thayumanavan, S. Noncovalent Encapsulation Stabilities in Supramolecular Nanoassemblies. *J. Am. Chem. Soc.* **2010**, *132*, 10683–10685.
- (27) Ryu, J. H.; Chacko, R. T.; Jiwanich, S.; Bickerton, S.; Babu, R. P.; Thayumanavan, S. Self-Cross-Linked Polymer Nanogels: A Versatile Nanoscopic Drug Delivery Platform. *J. Am. Chem. Soc.* **2010**, *132*, 17227–17235.
- (28) Gonzalez-Toro, D. C.; Ryu, J. H.; Chacko, R. T.; Zhuang, J. M.; Thayumanavan, S. Concurrent Binding and Delivery of Proteins and Lipophilic Small Molecules Using Polymeric Nanogels. *J. Am. Chem. Soc.* **2012**, *134*, 6964–6967.
- (29) Song, N.; Liu, W. M.; Tu, Q.; Liu, R.; Zhang, Y. R.; Wang, J. Y. Preparation and in Vitro Properties of Redox-Responsive Polymeric Nanoparticles for Paclitaxel Delivery. *Colloids Surf., B* **2011**, *87*, 454–463.
- (30) Wen, H. Y.; Dong, H. Q.; Xie, W. J.; Li, Y. Y.; Wang, K.; Pauletti, G. M.; Shi, D. L. Rapidly Disassembling Nanomicelles with Disulfide-Linked PEG Shells for Glutathione-Mediated Intracellular Drug Delivery. *Chem. Commun.* **2011**, *47*, 3550–3552.
- (31) Lee, S. Y.; Kim, S.; Tyler, J. Y.; Park, K.; Cheng, J. X. Blood-Stable, Tumor-Adaptable Disulfide Bonded mPEG-(Cys)₄-PDLLA Micelles for Chemotherapy. *Biomaterials* **2013**, *34*, 552–561.
- (32) Lee, S. Y.; Tyler, J. Y.; Kim, S.; Park, K.; Cheng, J. X. FRET Imaging Reveals Different Cellular Entry Routes of Self-Assembled and Disulfide Bonded Polymeric Micelles. *Mol. Pharmaceutics* **2013**, *10*, 3497–3506.
- (33) Brülisauer, L.; Gauthier, M. A.; Leroux, J. C. Disulfide-Containing Parenteral Delivery Systems and Their Redox-Biological Fate. *J. Controlled Release* **2014**, *195*, 147–154.
- (34) Cai, M. T.; Zhu, K.; Qiu, Y. B.; Liu, X. R.; Chen, Y. W.; Luo, X. L. pH and Redox-Responsive Mixed Micelles for Enhanced Intracellular Drug Release. *Colloids Surf., B* **2014**, *116*, 424–431.
- (35) Chiang, Y. T.; Yen, Y. W.; Lo, C. L. Reactive Oxygen Species and Glutathione Dual Redox-Responsive Micelles for Selective Cytotoxicity of Cancer. *Biomaterials* **2015**, *61*, 150–161.
- (36) Curcio, M.; Blanco-Fernandez, B.; Diaz-Gomez, L.; Concheiro, A.; Alvarez-Lorenzo, C. Hydrophobically Modified Keratin Vesicles for GSH-Responsive Intracellular Drug Release. *Bioconjugate Chem.* **2015**, *26*, 1900–1907.
- (37) Yu, D. H.; Zou, G. Y.; Cui, X. J.; Mao, Z. W.; Estrela-Lopis, I.; Donath, E.; Gao, C. Y. Monitoring the Intracellular Transformation Process of Surface-Cleavable PLGA Particles Containing Disulfide Bonds by Fluorescence Resonance Energy Transfer. *J. Mater. Chem. B* **2015**, *3*, 8865–8873.
- (38) Cao, S. P.; Pei, Z. C.; Xu, Y. Q.; Pei, Y. X. Glyco-Nanovesicles with Activatable Near-Infrared Probes for Real-Time Monitoring of Drug Release and Targeted Delivery. *Chem. Mater.* **2016**, *28*, 4501–4506.
- (39) Zhao, C. L.; Wang, Y. C.; Hruska, Z.; Winnik, M. A. Molecular Aspects of Latex Film Formation: an Energy-Transfer Study. *Macromolecules* **1990**, *23*, 4082–4087.
- (40) Ni, S. R.; Zhang, P.; Wang, Y. C.; Winnik, M. A. Energy Transfer Studies of the Boundary Layer Interphase in Polystyrene-Poly(methyl methacrylate) Block Copolymer Films. *Macromolecules* **1994**, *27*, 5742–5750.
- (41) Lakowicz, J. R. *Principles of Fluorescence Spectroscopy*, 3rd ed.; Springer: New York, 2006; pp 443–475.
- (42) Chen, H. T.; Kim, S. W.; He, W.; Wang, H. F.; Low, P. S.; Park, K.; Cheng, J. X. Fast Release of Lipophilic Agents from Circulating PEG-PDLLA Micelles Revealed by in Vivo Förster Resonance Energy Transfer Imaging. *Langmuir* **2008**, *24*, 5213–5217.
- (43) Chen, H. T.; Kim, S. W.; Li, L.; Wang, S. Y.; Park, K.; Cheng, J. X. Release of Hydrophobic Molecules from Polymer Micelles into Cell Membranes Revealed by Förster Resonance Energy Transfer Imaging. *Proc. Natl. Acad. Sci. U. S. A.* **2008**, *105*, 6596–6601.
- (44) Bickerton, S.; Jiwanich, S.; Thayumanavan, S. Interconnected Roles of Scaffold Hydrophobicity, Drug Loading, and Encapsulation Stability in Polymeric Nanocarriers. *Mol. Pharmaceutics* **2012**, *9*, 3569–3578.
- (45) Li, L. Y.; Thayumanavan, S. Environment-Dependent Guest Exchange in Supramolecular Hosts. *Langmuir* **2014**, *30*, 12384–12390.
- (46) Diezi, T. A.; Bae, Y.; Kwon, G. S. Enhanced Stability of PEG-block-poly(*N*-hexyl stearate 1-aspartamide) Micelles in the Presence of Serum Proteins. *Mol. Pharmaceutics* **2010**, *7*, 1355–1360.
- (47) Lu, J.; Owen, S. C.; Shoichet, M. S. Stability of Self-Assembled Polymeric Micelles in Serum. *Macromolecules* **2011**, *44*, 6002–6008.
- (48) Dong, H.; Dube, N.; Shu, J. Y.; Seo, J. W.; Mahakian, L. M.; Ferrara, K. W.; Xu, T. Long-Circulating 15 nm Micelles Based on Amphiphilic 3-Helix Peptide-PEG Conjugates. *ACS Nano* **2012**, *6*, 5320–5329.
- (49) Li, C. H.; Hu, J. M.; Liu, S. Y. Engineering FRET Processes within Synthetic Polymers, Polymeric Assemblies and Nanoparticles via Modulating Spatial Distribution of Fluorescent Donors and Acceptors. *Soft Matter* **2012**, *8*, 7096–7102.
- (50) Wang, J.; Wang, Y. G.; Liang, W. Delivery of Drugs to Cell Membranes by Encapsulation in PEG-PE Micelles. *J. Controlled Release* **2012**, *160*, 637–651.
- (51) Zou, P.; Chen, H. W.; Paholak, H. J.; Sun, D. X. Noninvasive Fluorescence Resonance Energy Transfer Imaging of in Vivo Premature Drug Release from Polymeric Nanoparticles. *Mol. Pharmaceutics* **2013**, *10*, 4185–4194.
- (52) Bastiat, G.; Pritz, C.; Roider, C.; Fouchet, F.; Lignieres, E.; Jesacher, A.; Glueckert, R.; Ritsch-Marte, M.; Schrott-Fischer, A.; Saulnier, P.; et al. A New Tool to Ensure the Fluorescent Dye Labeling Stability of Nanocarriers: a Real Challenge for Fluorescence Imaging. *J. Controlled Release* **2013**, *170*, 334–342.
- (53) Dan, K.; Ghosh, S. One-Pot Synthesis of an Acid-Labile Amphiphilic Triblock Copolymer and its pH-Responsive Vesicular Assembly. *Angew. Chem., Int. Ed.* **2013**, *52*, 7300–7305.
- (54) Gravier, J.; Sancey, L.; Hirsjärvi, S.; Rustique, E.; Passirani, C.; Benoit, J. P.; Coll, J. L.; Texier, I. FRET Imaging Approaches for in Vitro and in Vivo Characterization of Synthetic Lipid Nanoparticles. *Mol. Pharmaceutics* **2014**, *11*, 3133–3144.
- (55) Lainé, A. L.; Gravier, J.; Henry, M.; Sancey, L.; Bejaud, J.; Pancani, E.; Wiber, M.; Texier, I.; Coll, J. L.; Benoit, J. P.; et al. Conventional versus Stealth Lipid Nanoparticles: Formulation and in Vivo Fate Prediction through FRET Monitoring. *J. Controlled Release* **2014**, *188*, 1–8.
- (56) Xie, M.; Wang, S.; Singh, A.; Cooksey, T. J.; Marquez, M. D.; Bhattarai, A.; Kourentzi, K.; Robertson, M. L. Fluorophore Exchange Kinetics in Block Copolymer Micelles with Varying Solvent-Fluorophore and Solvent-Polymer Interactions. *Soft Matter* **2016**, *12*, 6196–6205.
- (57) Zhao, Y. M.; Fay, F.; Hak, S.; Manuel Perez-Aguilar, J.; Sanchez-Gaytan, B. L.; Goode, B.; Duivenvoorden, R.; de Lange Davies, C.; Bjørkøy, A.; Weinstein, H.; et al. Augmenting Drug-Carrier Compatibility Improves Tumour Nanotherapy Efficacy. *Nat. Commun.* **2016**, *7*, 1–11.
- (58) Ostaci, R. V.; Dameron, D.; Capponi, S.; Vignaud, G.; Léger, L.; Grohens, Y.; Drockenmüller, E. Polymer Brushes Grafted to “Passivated” Silicon Substrates Using Click Chemistry. *Langmuir* **2008**, *24*, 2732–2739.
- (59) Li, Y. J.; Hoskins, J. N.; Sreerama, S. G.; Grayson, S. M. MALDI-TOF Mass Spectral Characterization of Polymers Containing an Azide Group: Evidence of Metastable Ions. *Macromolecules* **2010**, *43*, 6225–6228.
- (60) Li, L. W.; Wang, X.; Yang, J. X.; Ye, X. D.; Wu, C. Degradation Kinetics of Model Hyperbranched Chains with Uniform Subchains and Controlled Locations of Cleavable Disulfide Linkages. *Macromolecules* **2014**, *47*, 650–658.

(61) Yang, J. X.; Li, L. W.; Jing, Z. Y.; Ye, X. D.; Wu, C. Construction and Properties of Hyperbranched Block Copolymer with Independently Adjustable Heterosubchains. *Macromolecules* **2014**, *47*, 8437–8445.

(62) Bock, V. D.; Hiemstra, H.; van Maarseveen, J. H. Cu^I-Catalyzed Alkyne-Azide “Click” Cycloadditions from a Mechanistic and Synthetic Perspective. *Eur. J. Org. Chem.* **2006**, *2006*, 51–68.

(63) Gou, P. F.; Zhu, W. P.; Shen, Z. Q. Synthesis, Self-Assembly, and Drug-Loading Capacity of Well-Defined Cyclodextrin-Centered Drug-Conjugated Amphiphilic A₁₄B₇ Miktoarm Star Copolymers Based on Poly(ϵ -caprolactone) and Poly(ethylene glycol). *Biomacromolecules* **2010**, *11*, 934–943.

(64) Yang, L. P.; Dong, X. H.; Pan, C. Y. Synthesis of Inverse Star Block Copolymer by Combination of ATRP, Ring Opening Polymerization, and “Click Chemistry”. *J. Polym. Sci., Part A: Polym. Chem.* **2008**, *46*, 7757–7772.

(65) Kim, S. H.; Tan, J. P.; Fukushima, K.; Nederberg, F.; Yang, Y. Y.; Waymouth, R. M.; Hedrick, J. L. Thermoresponsive Nanostructured Polycarbonate Block Copolymers as Biodegradable Therapeutic Delivery Carriers. *Biomaterials* **2011**, *32*, 5505–5514.

(66) Mahmud, A.; Lavasanifar, A. The Effect of Block Copolymer Structure on the Internalization of Polymeric Micelles by Human Breast Cancer Cells. *Colloids Surf., B* **2005**, *45*, 82–89.

(67) Zhang, Z.; Qu, Q. Q.; Li, J. R.; Zhou, S. B. The Effect of the Hydrophilic/hydrophobic Ratio of Polymeric Micelles on Their Endocytosis Pathways into Cells. *Macromol. Biosci.* **2013**, *13*, 789–798.

(68) Du, X. J.; Wang, J. L.; Liu, W. W.; Yang, J. X.; Sun, C. Y.; Sun, R.; Li, H. J.; Shen, S.; Luo, Y. L.; Ye, X. D.; et al. Regulating the Surface Poly(ethylene glycol) Density of Polymeric Nanoparticles and Evaluating its Role in Drug Delivery in Vivo. *Biomaterials* **2015**, *69*, 1–11.

(69) Yefimova, S. L.; Gural'chuk, G. Y.; Sorokin, A. V.; Malyukin, Y. V.; Borovoy, I. A.; Lubyayaya, A. S. Hydrophobicity Effect on Interactions between Organic Molecules in Nanocages of Surfactant Micelle. *J. Appl. Spectrosc.* **2008**, *75*, 658–663.

(70) Broussard, J. A.; Rappaz, B.; Webb, D. J.; Brown, C. M. Fluorescence Resonance Energy Transfer Microscopy as Demonstrated by Measuring the Activation of the Serine/threonine Kinase Akt. *Nat. Protoc.* **2013**, *8*, 265–281.

(71) Weitz, D. A.; Huang, J. S.; Lin, M. Y.; Sung, J. Dynamics of Diffusion-Limited Kinetic Aggregation. *Phys. Rev. Lett.* **1984**, *53*, 1657–1660.

(72) Sabin, J.; Prieto, G.; Sarmiento, F. Stable Clusters in Liposomic Systems. *Soft Matter* **2012**, *8*, 3212–3222.

(73) Lu, Y. J.; Ye, X. D.; Zhou, K. J.; Shi, W. J. A Comparative Study of Urea-Induced Aggregation of Collapsed Poly(*N*-isopropylacrylamide) and Poly(*N,N*-diethylacrylamide) Chains in Aqueous Solutions. *J. Phys. Chem. B* **2013**, *117*, 7481–7488.

(74) Choi, S. H.; Lodge, T. P.; Bates, F. S. Mechanism of Molecular Exchange in Diblock Copolymer Micelles: Hypersensitivity to Core Chain Length. *Phys. Rev. Lett.* **2010**, *104*, 047802.

(75) Win, K. Y.; Feng, S. S. Effects of Particle Size and Surface Coating on Cellular Uptake of Polymeric Nanoparticles for Oral Delivery of Anticancer Drugs. *Biomaterials* **2005**, *26*, 2713–2722.